

Research papers

Hybrid energy storage system and management strategy for motor drive with high torque overload

Ze Wang^{a,b,*}, Jiahe Li^{a,b}, Chuxiong Hu^{a,b}, Xiong Li^c, Yu Zhu^{a,b}

^a Department of Mechanical Engineering, Tsinghua University, Beijing, China

^b Beijing Key Lab of Precision/Ultra-Precision Manufacture Equipments and Control, Tsinghua University, Beijing, China

^c Tencent Robotics X Lab, Shenzhen, China



ARTICLE INFO

Keywords:

Battery–supercapacitor hybrid energy storage system (BSHES)
Bidirectional DC converter (BDC)
Energy management strategy
Torque overload

ABSTRACT

The demand for small-size motors with large output torque in fields such as mobile robotics is increasing, necessitating mobile power systems with greater output power and current within a specific volume and weight. However, conventional mobile power sources like lithium batteries face challenges in surpassing the dual limitations of weight and output power due to constraints imposed by materials and other factors. Therefore, this paper references the approach of high-power hybrid energy systems in automobiles and proposes a battery–supercapacitor hybrid energy storage system (BSHES) and energy management strategy. The motor is powered by the battery during low torque operating conditions, while the additional output power of the battery is used to charge the supercapacitor. In cases of torque overload, the rapid discharge of the supercapacitor provides the motor with a high current, ensuring instantaneous high output power. Furthermore, the proposed energy management strategy is used to control the charging and discharging processes of the supercapacitor, guaranteeing that the charging process of the supercapacitor does not interfere with the battery's power supply to the motor, as well as maintaining controllability and stability of the current in the discharge process. The feasibility of the principle is verified through simulations, and we also design a complete prototype of the proposed BSHES and conduct experiments on the motor. The results demonstrate that the maximum output current to the motor is increased by 150% compared to the original level, and the weight is reduced by 64.7% compared to a pure battery-powered system with same maximum current output. Additionally, the energy management strategy enables a more stable charging and discharging process compared to the unmanaged state.

1. Introduction

The high-performance servo drive systems, characterized by high precision, fast response and large torque, have been extensively utilized in many fields, such as robotics, aerospace, etc [1,2]. As the requirement for small self-weight and the demand for output precision grows higher, the direct-drive motor is gradually replacing the conventional combination of motors and transmission systems, emerging as a novel servo-drive mode [3,4]. While direct-drive motors can effectively avoid motion errors caused by transmission components and noticeably reduce the volume of the motor system, they simultaneously lose the torque amplification capability offered by the transmission mechanism. Although certain direct-drive motors can achieve an output torque exceeding 20 Nm, they necessitate power supplies capable of delivering an output power of over 1.5 kW [5], which is considerably higher than the requirements of non-direct-drive motors for the output power system. The application scenarios of mobile robots are significantly

different from those of vehicles and fixed mounted industrial manipulators, imposing relatively strict requirements on the weight and volume of power supply. However, these requirements clearly contradict the demand for high output power. As a result, conventional single-form power sources like lithium batteries struggle to accommodate the need for lightweight, compact design and high output power. Hence, hybrid energy storage systems have emerged as a crucial solution to tackle this problem.

Several studies show that supercapacitors (SCs) can store and discharge high currents rapidly. As a result, SCs have found applications in various fields, such as hybrid energy vehicles, solar energy systems, and wind power generation. Leveraging this unique property of SCs, research on battery–supercapacitor hybrid energy storage systems (BSHES) comprising lithium batteries has garnered significant attention in several domains. Various research show that the BSHES system exhibits outstanding performance under appropriate control [6,

* Corresponding author at: Department of Mechanical Engineering, Tsinghua University, Beijing, China.

E-mail address: wangze20@tsinghua.edu.cn (Z. Wang).

7]. Utilizing supercapacitors (SCs) in this system alleviates the output burden on the battery [8,9], safeguarding it against surge impacts and extending its lifespan. Moreover, SCs can serve as auxiliary power sources in scenarios with high power demands [10,11], resulting in reduced system size and weight [12]. These advantages underscore the efficacy of integrating SCs into the BSHESS framework.

One typical application scenario of the BSHESS is hybrid energy vehicles (HEV). Numerous studies have been conducted to leverage the properties of supercapacitors (SCs), such as fast response time, long operational lifespan, and high energy density [13,14], in order to achieve a smooth discharge current of HEV batteries [15] and enhance the peak power capabilities of the power supply system [16]. Additionally, researchers have explored SC-based energy recovery methods [17]. Prototypes have been designed for verification purposes, and experimental results demonstrate that the proposed energy management strategy effectively controls energy flow, satisfying the transient high-power demands of the vehicle. This strategy successfully achieves goals such as smoothing battery current, and reducing the frequency of charge and discharge cycles, thereby extending battery life [18].

The key aspect of BSHESS lies in the synergistic management of the voltage levels of the battery and SC. Due to the substantial voltage disparity between the battery and supercapacitor in normal operating conditions, a bidirectional DC converter (BDC) is typically employed to connect the two, ensuring the proper operation of the BSHESS system [19]. Therefore, the design and control strategy of the BDC are crucial for achieving efficient energy management. The structure of the BDC varies significantly depending on the specific form of the energy management system being utilized. Typically, during the charging process of the SC, the BDC operates in buck mode. Conversely, during the discharging process of the SC, the BDC functions in boost mode. To maintain a consistent voltage level during SC discharging, some researchers have proposed a bi-directional quasi-Z-source inverter (qZSI) based BDC for SC interfacing in high-power applications [20]. Several studies have demonstrated that the qZS network can serve as a low-pass filter during the charging mode, effectively smoothing the charging current of the supercapacitors while avoiding sudden fluctuations in battery voltage and current [21]. Furthermore, certain studies have introduced a hybrid circuit structure, aiming to optimize the number of BDC components and enhance system reliability. The proposed control scheme has been validated through theoretical analysis and experimental verification [22].

In addition, the optimization of the switch circuit is another important area of research in BDC development. Some studies have explored the implementation of soft-switching techniques by incorporating additional components such as inductors and capacitors [23,24]. These approaches aim to achieve zero-current turn-off and zero-voltage turn-on of the switch circuit [25,26], thereby enhancing energy flow efficiency [27]. It has been observed that the soft-switching mode is more suitable for the heavy loads, while the hard-switching mode is more appropriate for the light-load conditions [28]. Building upon the original soft-switch circuit, certain studies have managed to reduce the number of extra components at the expense of a slight decrease in energy flow efficiency, resulting in a significant improvement in system reliability. Moreover, the proposed soft-switch circuit still exhibits substantial enhancement in energy flow efficiency compared to the conventional hard-switch circuit [29].

Although BSHESS has been widely applied in high-power supply systems, there have been few studies considering its use in relatively low-power (<5 kW) servo motors. Building upon the previous discussion on the demand for high-performance power supply systems for direct-drive motors, this paper innovatively proposes a BSHESS and its energy management strategy specifically designed for small motors. Different from other mature research works, this study focuses more on the motor's instantaneous torque overload capacity and the self-weight of the power supply system. To address this demand, a novel BDC structure is proposed in this paper, which ensures that the BSHESS can

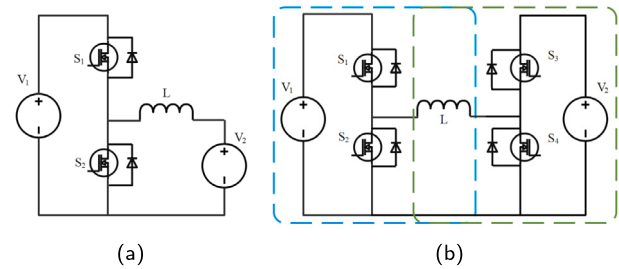


Fig. 1. Simplified circuits structure. (a) Single Buck-Boost unit. (b) The proposed BDC.

achieve the following three functions with a simple circuit topology: (1) battery-powered motor under normal load torque (same as the single battery power mode); (2) simultaneous battery power to the motor and utilization of surplus power to charge the SC without interfering with the motor operation; (3) collaborative power supply to the motor by both the SC and the battery under torque overload conditions, with adjustable and controllable supply current. The subsequent Section 2 introduces the implementation principle and simulation of the energy management system, specific energy management strategies are provided in Section 3, and experimental verification of the charging and discharging processes are presented in Section 4. The experimental results fully confirm that the SC charging process has no impact on the normal operation of the motor, and the maximum output current during discharge can be increased by up to 133.3%. Detailed introduction and supplementary videos are provided in the following sections for readers' reference.

2. Principle analysis and simulation

2.1. Generalized form

Structure of BDC proposed in this paper is shown in Fig. 1(b). As it can be seen, the whole BDC structure is formed by two separate Buck-Boost circuits in Fig. 1(a) connected in reverse. By proper control of the switches S_1 - S_4 of the converter, bidirectional flow of energy and voltage rise and fall function can be available at the two sides.

2.2. Topology analysis

To explain further, let us consider single Buck-Boost unit at first, through which voltage rise and voltage fall function is available at two different directions. Single Buck-Boost unit has two operations: the positive operation and the negative operation. The energy flows from the high side (V_1) to the low side (V_2) in the positive operation, and the Buck-Boost unit works at the Buck mode. The energy flows from the low side (V_2) to the high side (V_1) in the negative operation, and the Buck-Boost unit works at the Boost mode. The main circuit of the topology is composed of switches S_1 , S_2 , the main inductor L, and voltage sources V_1 , V_2 . The positive operation can be regarded as the Buck mode, in which the energy flows from the high side to the low side. Considering that the ratio of voltage on V_1 side and voltage on V_2 side is transformer multiple M, M can be calculated as

$$M = \frac{V_1}{V_2}. \quad (1)$$

D represents the duty cycle of the control pulse width modulation (PWM) signal for S_1 . Working state in positive operation of the buck-boost unit can be divided into two modes, and in every mode, current of the main inductor (i_L) is positive and continuous. The analysis about every mode is given as follows.

Mode 1: In single switching period T, S_1 is turned on first. Then because voltage of V_1 is larger than V_2 , the current will flow as shown

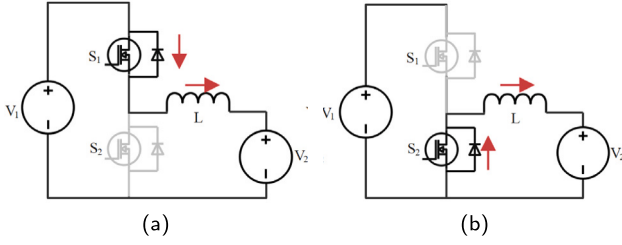


Fig. 2. Operating modes analysis in the positive operation of single Buck-Boost unit. (a) Mode 1. (b) Mode 2.

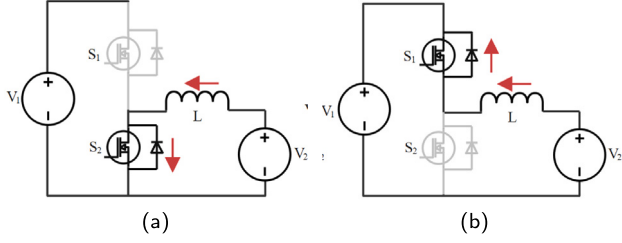


Fig. 3. Operating modes analysis in the negative operation of single Buck-Boost unit. (a) Mode 1. (b) Mode 2.

in Fig. 2(a). The increase of current of main inductor L can be calculated as

$$\Delta i_{L(+)} = \int_0^{t_1} \frac{V_1 - V_2}{L} dt = \frac{V_1 - V_2}{L} DT. \quad (2)$$

Mode 2: After Mode 1, S_1 is turned off. Then the current will flow as shown in Fig. 2(b). The decrease of current of main inductor L can be calculated as

$$\Delta i_{L(-)} = \int_{t_1}^{t_2} \frac{V_2}{L} dt = \frac{V_2}{L} (1 - D)T. \quad (3)$$

Because current of the main inductor L is positive and continuous, Then

$$\Delta i_{L(+)} = \Delta i_{L(-)}. \quad (4)$$

Based on (1)-(4), transformer multiple M of the positive operation can be calculated as

$$M = \frac{V_1}{V_2} = D. \quad (5)$$

The negative operation can be regarded as the Boost mode, in which the energy flows from the low side to the high side. D represents the duty cycle of the control pulse width modulation (PWM) signal for S_2 . Working state in negative operation of the buck-boost unit can be divided into two modes. Also, in every mode, i_L is positive and continuous. The analysis about every mode is given as follows.

Mode 1: In single switching period T, S_2 is turned on. Then the current will flow as shown in Fig. 3(a). The increase of current of main inductor L can be calculated as

$$\Delta i_{L(+)} = \int_0^{t_1} \frac{V_2}{L} dt = \frac{V_2}{L} DT. \quad (6)$$

Mode 2: After Mode 1, S_2 is turned off. Then the current will flow As shown in Fig. 3(b). The decrease of current of main inductor L can be calculated as

$$\Delta i_{L(-)} = \int_{t_1}^{t_2} \frac{V_1 - V_2}{L} dt = \frac{V_1 - V_2}{L} (1 - D)T. \quad (7)$$

Because current of the main inductor L is positive and continuous, Then

$$\Delta i_{L(+)} = \Delta i_{L(-)}. \quad (8)$$

Based on (1)-(4), transformer multiple M of the positive operation can be calculated as

$$M = \frac{V_1}{V_2} = 1 - D. \quad (9)$$

Both positive operation and negative operation are expected to work at the continuous conduction mode (CCM), in which the parameters of some components are required to be set. From (2)(3)(6)(7), we know that in a single switching period T, the current of main inductor L will increase or decrease first and decrease or increase after that. Therefore, in CCM, the minimum current of main inductor L, can be calculated as

$$I_{Lmin} = I_O - \frac{\Delta i_{L(-)}}{2} \geq 0. \quad (10)$$

Based on (3)(10), the decrease of current of the main inductor L in positive operation is required to be less than

$$\Delta i_{L(-)} = \int_{t_1}^{t_2} \frac{V_2}{L} dt = \frac{V_2}{L} (1 - D)T \leq 2I_O. \quad (11)$$

Also based on (7)(10), the decrease of current of the main inductor L in negative operation is required to be less than

$$\Delta i_{L(-)} = \int_{t_1}^{t_2} \frac{V_1 - V_2}{L} dt = \frac{V_1 - V_2}{L} (1 - D)T \leq 2I_L. \quad (12)$$

Because there are output current I_O only in mode2 of negative operation, output current I_O can be calculated as

$$I_O = I_L(1 - D). \quad (13)$$

Then we get the minimum main inductor L of positive operation and negative operation.

$$L \geq \frac{V_2}{2I_O} (1 - D)T. \quad (14)$$

$$L \geq \frac{V_2}{2I_O} D(1 - D)^2T. \quad (15)$$

Moreover, filter capacitor can also be determined by the similar principle, in which the voltage ripple can be calculated as

$$\Delta V_C = \frac{1}{C} \int_0^{\frac{T}{2}} i_{cf} dt. \quad (16)$$

Then filter capacitor of positive and negative operation can be calculated as

$$C \geq \frac{\Delta i_L}{8\Delta V_C f} = \frac{(V_1 - V_2)D}{8L\Delta V_C f^2}. \quad (17)$$

$$C \geq \frac{I_O D}{\Delta V_C f}. \quad (18)$$

Because the proposed BDC is formed by two separate Buck-Boost units connected in reverse, and one side is connected with battery with voltage V_B and the other side is connected with SC with voltage V_C , transformer multiple M of the BDC can be calculated as

$$M = \frac{V_C}{V_B} = \frac{D_1}{D_2}. \quad (19)$$

2.3. Simulation analysis

To verify the proposed BDC structure, Simulations has been done in two cases: forward operation, in which current flows from V_1 side with lower voltage to V_2 side with higher voltage, and opposite operation, in which current flows from V_2 side with lower voltage to V_1 side with higher voltage. Every cases has three modes, in which gate voltages of Mosfet ($V_{G1}, V_{G2}, V_{G3}, V_{G4}$), drain-source voltages of Mosfet ($V_{S1}, V_{S2}, V_{S3}, V_{S4}$), drain-source currents ($i_{S1}, i_{S2}, i_{S3}, i_{S4}$) and current of the main inductor (i_L) changes (see Table 1).

In forward operation, as shown in Fig. 4, with changing of wave-forms of $V_{G1} - V_{G4}$, $V_{S1} - V_{S4}$ changes. Also, $i_{S1} - i_{S4}$ and i_L changes. The analysis about every mode is given as follows.

Table 1
Simulation parameters of the proposed BDC.

Parameter	Term used	Value
Battery	DC Voltage Source	30 V
Supercapacitor	Series RLC Branch (RC)	54 F, 40 mΩ (IR)
Power Inductors	Series RLC Branch (RL)	47 μH, 12 mΩ (IR)
Filter Capacitor	Series RLC Branch (C)	300 μF
S_1 - S_4	Mosfet	1.3 V (IDFV)
Control Signal	Pulse Generator	Q_1, Q_3, T

IDFV = Internal diode forward voltage V_f;

IR = Internal resistance

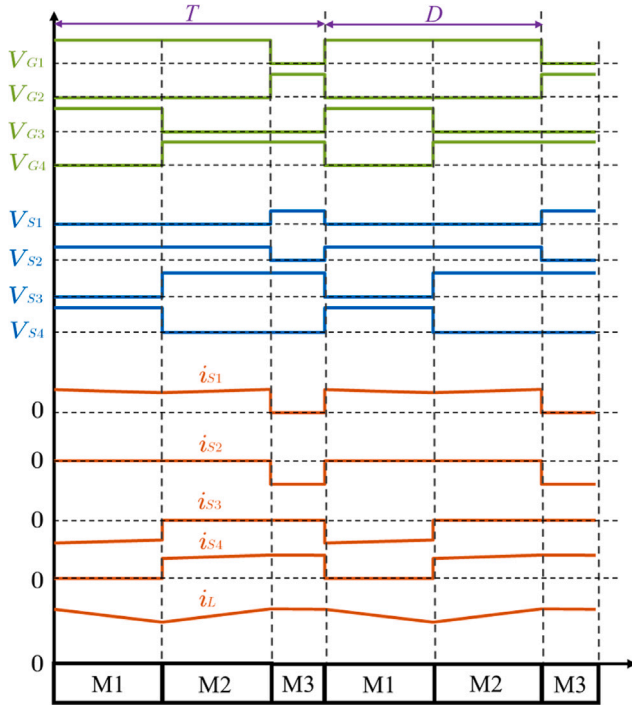


Fig. 4. Simulation images of forward operation.

Mode 1: S_1 and S_3 are conducting. Because current of the main inductor L is positive and flows from its left to its right, the current flows from V_1 to V_2 . And because the voltage of V_2 is higher than the voltage of V_1 , i_L gets lower in this mode. Therefore, i_{S1} and i_{S3} get lower.

Mode 2: S_1 and S_4 are conducting. In this mode, the voltage of V_1 is applied to both ends of L, so i_L gets higher, and i_{S1} and i_{S4} get higher.

Mode 3: S_2 and S_4 are conducting. The voltage applied to both ends of L is 0, so i_L gets lower slowly. At the same time, i_{S2} and i_{S4} get lower.

In opposite operation, as shown in Fig. 5, the analysis is also given as follows.

Mode 1: S_1 and S_3 are conducting. Because current of the main inductor L is negative and flows from its right to its left, the current flows from V_2 to V_1 . And because the voltage of V_1 is higher than the voltage of V_2 , i_L gets lower in this mode. Therefore, i_{S1} and i_{S3} get lower.

Mode 2: S_2 and S_3 are conducting. In this mode, the voltage of V_2 is applied to both ends of L, so i_L gets higher, and i_{S2} and i_{S3} get higher.

mode 3: S_2 and S_4 are conducting. The voltage applied to both ends of L is 0, so i_L gets lower slowly. At the same time, i_{S2} and i_{S4} get lower.

Simulation of charging SC with the proposed BDC is also done, as shown in Fig. 6. The control PWM signals for S_1 - S_4 are all fixed. It can be found by simulation images that the charging current of SC fluctuates greatly, which can be reduce through changing value of the main inductor and the filter capacitor. Moreover, output current

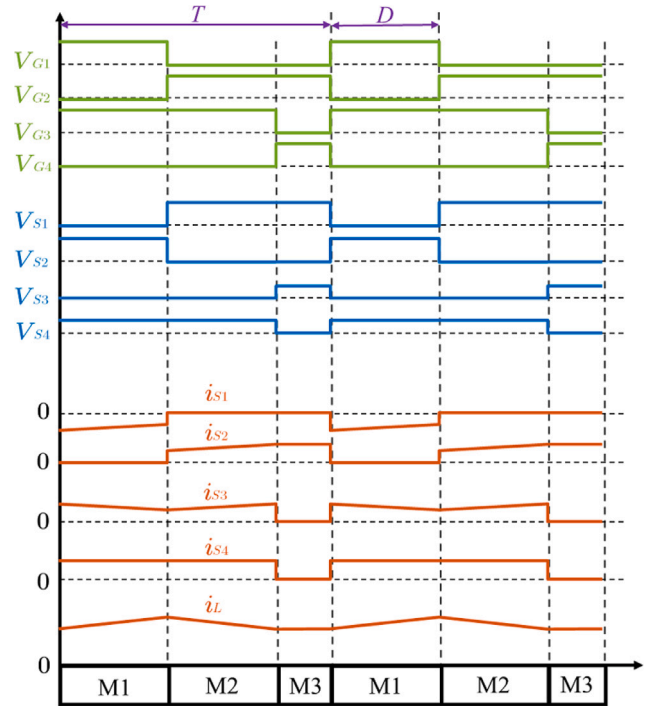


Fig. 5. Simulation images of opposite operation.

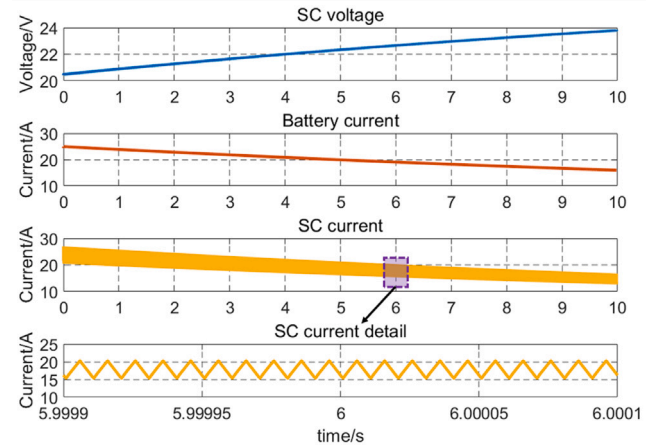


Fig. 6. Charging images of SC in a long period.

of battery, charging current of SC get low when voltage of SC gets high, which means that without change of PWM signals, charging speed of SC will become slow. Considering that charging speed of SC also cannot become too fast, which may interfere with the normal operation of motor, PWM signals are expected to be changed when the SC is charging.

3. Energy management strategy

3.1. Generalized principle

As shown in Fig. 7, the battery B is connected in parallel to the motor M, and then to the SC through BDC. After the full energy voltage of the SC (U_0) is calibrated and the current voltage of SC is measured, energy of SC (Q) and super capacitor state of charge (SOC) can be calculated as

$$Q = \frac{1}{2}CU^2. \quad (20)$$

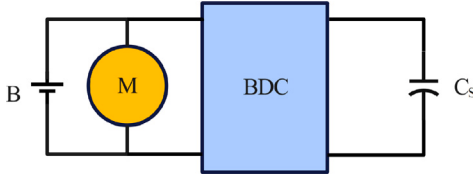


Fig. 7. BSHESS structure configuration.

$$SOC = \frac{Q}{Q_0} = \frac{\frac{1}{2}CU^2}{\frac{1}{2}CU_0^2} = \left(\frac{U}{U_0}\right)^2. \quad (21)$$

In order to guarantee the normal operation of motor circuit and make full use of the output capacity of battery, an energy management strategy is proposed in this section.

3.2. Charging principle

When motor works at low speed and low torque mode, there is overflow of output capacitor of battery, so the excess power is expected to be used in charging SC. Based on the analysis of the proposed BDC, transformer multiple M can be changed by changing D_1 and D_2 , and the charging current can be calculated as

$$I_C = \frac{V_C - U_C}{R_C}. \quad (22)$$

Based on (23), output voltage V_C of BDC in SC side, which can be changed by changing PWM D_1 and D_2 , has an effect on the value of the charging current I_C . Also, the internal resistance R_C and current voltage of the SC U_C have effect on I_C . The higher the I_C , the higher output current of battery I_B is. Therefore, charging principle of the proposed energy management strategy is: changing V_C and controlling the I_B below $I_{Bmax} - I_M$. I_{Bmax} is the maximum output current of battery and I_M is the demand current of motor.

3.3. Discharging principle

When motor works at high speed and high torque mode, there is extra requirements of power supply, so the SC is expected to offer extra power required. Based on the analysis of the proposed BDC, transformer multiple M can be changed by changing D_1 and D_2 , and the discharging current can be calculated as

$$I_M = \frac{V_B - U_M}{R_M}. \quad (23)$$

Based on (23), discharging principle of the proposed energy management strategy is: controlling the actual output current of BSHESS I_O and the demand current of motor I_M consistent and steady.

3.4. Control framework

As shown in Fig. 8, based on the above analysis of the charging principle and discharging principle of the proposed BSHESS, a control framework is proposed, including Charging and discharging determination, control loop of charging speed and control loop of discharging speed. In charging and discharging determination, according to the current voltage of SC and demand of motor, such as rotate speed controller choose to charging the SC or make SC discharge. In charging mode, controller set the target battery output current I_B' , which differs from sampling battery output current I_B^* . Then the PI feedback controller calculates the D_1, D_3 , which is the PWM parameters of S_1 and S_3 in the proposed BDC. In discharging mode, controller set the target BSHESS output current I_O' , which differs from sampling BSHESS output current I_O^* . Then the PI feedback controller also calculate the D_1, D_2 to control the switches in the proposed BDC.

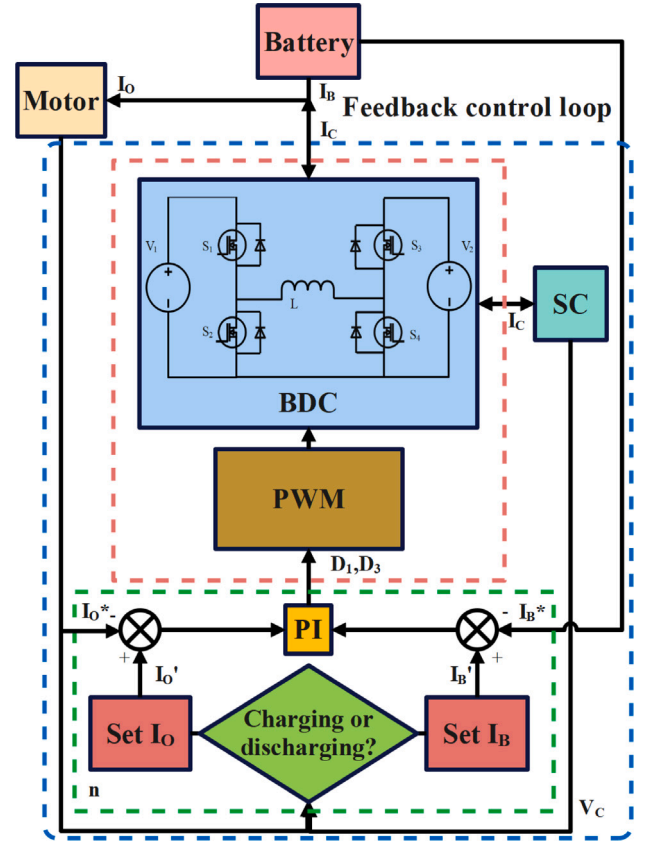


Fig. 8. Control framework diagram.

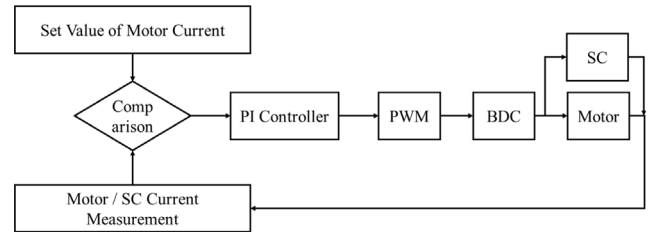


Fig. 9. Control logic and process.

Unlike other hybrid energy systems that focus on energy management itself, our control scheme prioritizes the actual operational performance of the motor. In the absence of control action in an open-loop system, the fluctuation in the charging and discharging rates of the supercapacitor is determined by its inherent characteristics. Therefore, during the charging process of the supercapacitor, our control strategy not only considers the charging rate but also focuses on the impact of the charging process on the smooth operation of the motor. The overall control logic and process can be further explained in Fig. 9. During the charging process of the supercapacitor, the current magnitude in the motor circuit is monitored. If a deviation is detected between the motor current and the set value, the PWM of the BDC switch is controlled by a PI controller to adjust the charging current of the supercapacitor. Similarly, during the discharging process of the supercapacitor, a similar approach is adopted to PI control the current input from the supercapacitor to the motor, avoiding both excessive current causing overshoot and insufficient current leading to insufficient power. Simultaneously, the discharge time and quantity of the supercapacitor are monitored, and if there is insufficient electrical energy, appropriate adjustments are made to the control task of the motor.

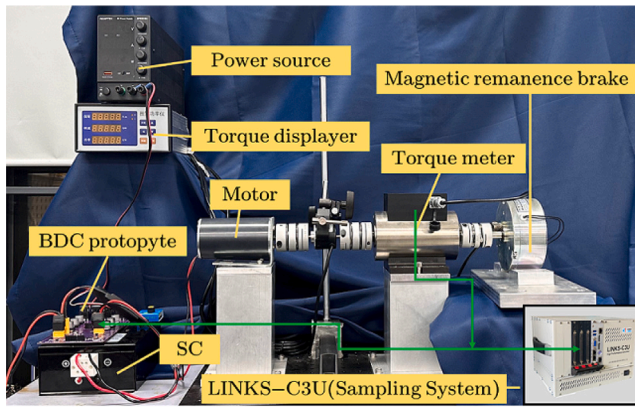


Fig. 10. Experimental BDC prototype and motor torque test bench.

Table 2

Experiment parameters of the proposed bshess prototype.

Parameter	Value
Battery	30 V, 8 A (max output current)
Supercapacitor	27 V (max voltage), 54 F, 40 mΩ (IR)
Power Inductors	47 μH, 12 mΩ (IR)
Filter Capacitor	300 μF
MOSFET	IRFP260NPBF
MOSFET Driver	UCC27211D

IR = Internal resistance.

4. Experimental results

4.1. Generalized experimental setup

In order to verify the proposed BDC and BSHESS, an experimental prototype is built based on the proposed BDC structure. And a motor torque test bench is built to test the output torque of motor, as shown in Fig. 10. The parameters of the components used in the experiment are shown in Table 2. Sampling system is LINKS-C3U, which is equipped with a multi-core CPU and an optional Simulink programmable FPGA that enables closed-loop sampling rates up to the MHz (microsecond) range. The Links-C3U supports up to 21 expansion slots, providing scalability to cover hundreds of I/O signals. In the experiments, the sampling period was set to be 0.01 s.

4.2. Charging mode

In the charging experiments, SC was first charging without control of charging speed, and then SC was charging with feedback control of charging speed.

The measured voltage waveform of Mosfet in BDC during charging process is shown in Fig. 11. The blue curve represents the drain–source voltage of the Mosfet, and the green one represents the gate voltage of the Mosfet. From the figure, it can be observed that in the experiment, effective control of the gate voltages of the Mosfet directly determines the on/off state of the BDC circuit, thereby validating the correctness of the designed BDC circuit structure.

When SC was charging without control, as shown in Fig. 12, output current of battery decrease gradually, causing charging speed of SC decrease. In Fig. 12(a), output current of battery is 8 A at first and the excess current of battery is 0, which limited current that the motor can use and affected the normal operation of the motor. Based on the fast and slow charging experiments of SC without control, a conclusion can be drawn: control of charging speed of SC is necessary to guarantee the SOC. In Fig. 12(b), output current of battery is 5 A at first, and nearly decreased to 3 A in the end. At the same time, the excess current of

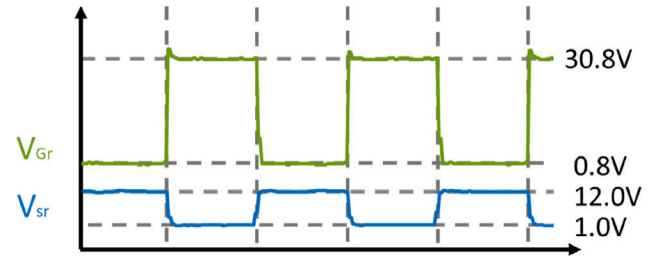


Fig. 11. Measured voltage of Mosfet during experiments. (For interpretation of the references to color in this figure legend, the reader is referred to the web version of this article.)

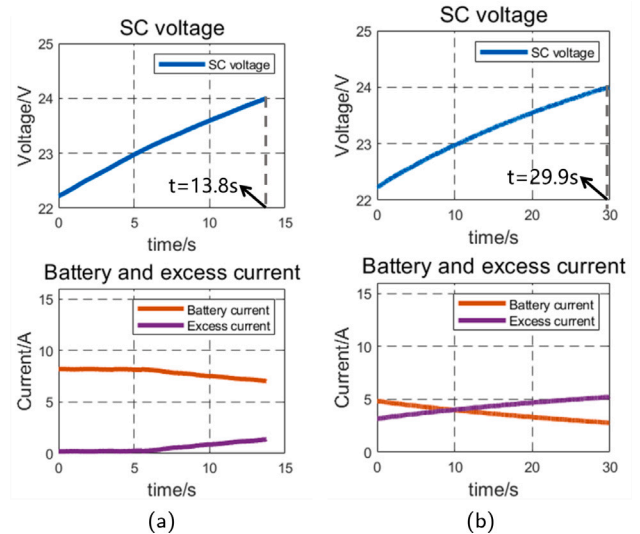


Fig. 12. Charging experiments of SC without control. (a) Fast charging images. (b) Slow charging images.

battery, which was not used for SC charging, increased from 3 A to 5 A. Therefore, the average charging speed of SC is too slow and there is still much current can be used for charging SC. To realize a fast charging speed, output current of battery are expected to be high at fist in this condition without control, which caused another problem.

When SC was charging with the proposed energy management strategy, as shown in Fig. 13, output current of battery is controlled by feedback control loop. According to the demand current of motor, output current of battery used to charge SC was kept steady in different value (3 A and 5 A). Therefore, the proposed strategy guaranteed the normal operation of motor.

4.3. Discharging mode

In the discharging experiments, SC first discharged without control of discharging speed. And then SC discharged with feedback control of discharging speed.

When SC discharged without control, as shown in Fig. 14, output current of BSHESS decrease gradually, causing output voltage and motor torque decrease. Fixed PWM signals cannot kept output of BSHESS steady when there is high output current of SC and decrease of voltage of SC. In Fig. 14(b), output current and voltage of BSHESS and motor torque decrease 25% in 8 s.

When SC discharged with the proposed energy management strategy, as shown in Figs. 15 and 16, output current of BSHESS is controlled by feedback control loop. According to the demand current of motor, output current of BSHESS kept steady in different value (15 A and 20 A), while guaranteeing the normal operation of motor.

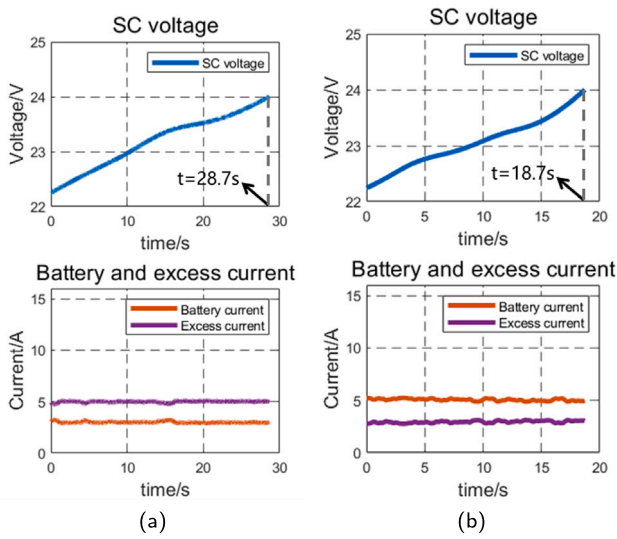


Fig. 13. Charging experiments of SC with control. (a) Charging images (3 A). (b) Charging images (5 A).

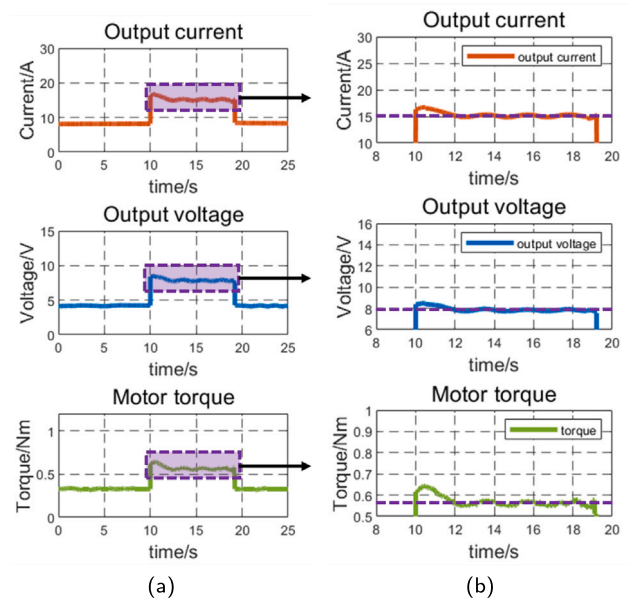


Fig. 15. Discharging experiments of SC with control in low current (15 A). (a) Output current and voltage of the proposed BSHESS and motor torque. (b) Detail of images when SC discharges.

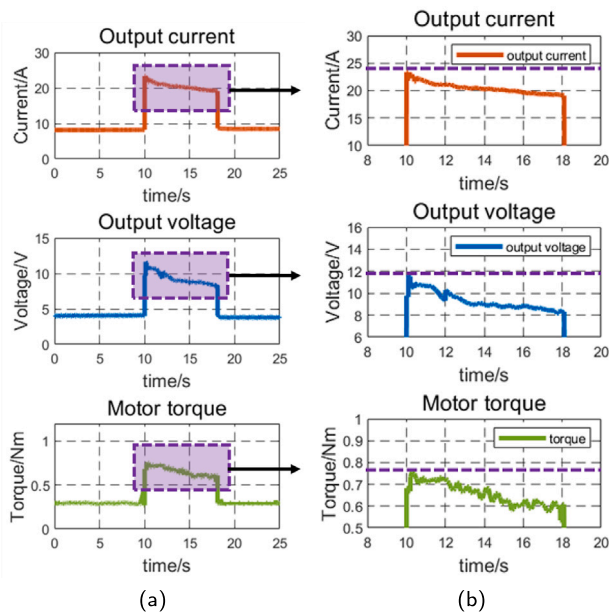


Fig. 14. Discharging experiments of SC without control. (a) Output current and voltage of the proposed BSHESS and motor torque. (b) Detail of images when SC discharges.

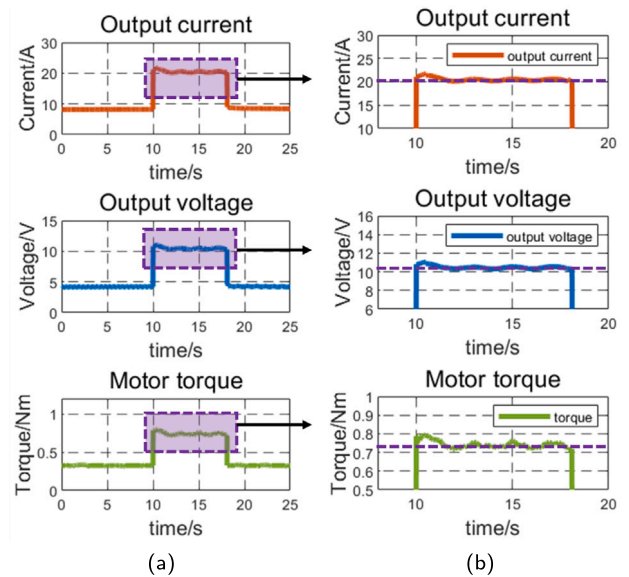


Fig. 16. Discharging experiments of SC with control in high current (20 A). (a) Output current and voltage of the proposed BSHESS and motor torque. (b) Detail of images when SC discharges.

Table 3

Prototype and single battery performance comparison table.

Comparison	Battery1	Battery2	BSHESS
Maxcurrent (A)	10	20	20
Volume (mm)	200*120*75	310*210*120	170*140*100
Weight (kg)	1.75	8.5	1
Model number	SHKS-24V	ACPB-24V	BSHESS

Weight and volume of the BSHESS does not include the experimental power source.

Based on the above experiments results, the proposed BSHESS can realize higher current output than single power source. In the experiments, single power source can only output 8 A current, as shown in the Table 2, and the proposed BSHESS can output 20 A current, as shown in Fig. 16, while there is still great output potential to be developed. In the Table 3, weight and volume of the BSHESS does not include the experimental power source, because weight and volume of power

source cannot be compared with battery directly. Compared with single battery 1, as shown in the Table 3, the proposed BSHESS increased the maximum current output capacity. We increased the maximum output current by 150%. Compared with single battery2, the proposed BSHESS has lighter weight. Even using battery1 instead of power source, the weight of the whole BSHESS will not exceed 3 kg, which means a weight reduction of 64.7%. Moreover, after improvement of structure of BSHESS in the future work, its volume and weight can be smaller.

4.4. Discussion

Compared with other relevant studies, the proposed BDC allows energy to flow in both directions, while allowing the voltage to be

changed in both directions. It means that there is a greater range of regulations for the proposed BDC. This characteristic can be compared with the basic circuit of a design called soft-switching, as mentioned in Ref. [29]. The basic circuit of soft-switching described in [29] can be considered as half of the proposed four-switch bidirectional BDC circuit in this paper. It enables a boost in one direction and a buck in the other direction. In contrast, the proposed BDC in this paper achieves bidirectional voltage conversion by connecting two individual BDCs in reverse. This allows for more flexible applications. However, with the greater range of regulation, the energy transfer efficiency of the proposed BDC might be a little lower than other BDCs. Because there are four switches in the proposed BDC, which means that there are two more switches than some relevant BDC, there will be some dissipation of energy on them. We believe that the issues of energy transfer efficiency can be effectively addressed through the optimization of the circuit system.

In the experiments, we use series resistance (0.1Ω or 1Ω) to measure the current of the proposed BDC. In the proposed BDC circuit, sometimes the current will be more than 15 A or even 30 A, so the energy loss on resistance is quite big. When calculating efficiency, we have tried to remove the effect of series resistance. Now the efficiency of the proposed BDC prototype is about 74%. Moreover, we have found that the efficiency will become lower in the SC charging mode when the voltage of the SC become higher. However, this method of calculation is not to our satisfaction, so we plan to improve the efficiency and measurement method in the future.

5. Conclusion

In this paper, we propose a novel BSHESS specifically designed for servo motors. The BSHESS combines the advantages of small volume, lightweight, and high power output in the power supply system by integrating batteries and supercapacitors. Additionally, we propose an energy management strategy tailored for BSHESS, ensuring that the supercapacitors utilize the residual power from the batteries to charge during normal torque conditions of the motor without affecting its normal operation. Moreover, this strategy effectively controls the discharge process of supercapacitors, ensuring precise and controllable high output currents. In addition, we also propose a complete prototype of BSHESS and conduct various charging and discharging experiments with the motor system. The results demonstrate a remarkable increase in the maximum output current by 150% compared to the single power supply mode. Furthermore, compared to a commercially available pure battery system with an equivalent maximum output current capability, a weight reduction of 64.7% is achieved. The proposed BSHESS and energy management strategy provide a new implementation approach for mobile power supply systems and offer possibilities for instant high-torque output in servo drive systems, particularly in scenarios involving mobile robots. This research carries significant application potential.

Declaration of competing interest

The authors declare the following financial interests/personal relationships which may be considered as potential competing interests: Ze Wang reports financial support was provided by National Natural Science Foundation of China and CIE-Tencent Robotics X Rhino-Bird Focused Research Program

Data availability

The data that has been used is confidential.

Acknowledgments

This work was supported by the National Nature Science Foundation of China under Grant 52205532 and CIE-Tencent Robotics X Rhino-Bird Focused Research Program.

Appendix A. Supplementary data

Supplementary material related to this article can be found online at <https://doi.org/10.1016/j.est.2023.109432>.

References

- [1] Yasser Abdel-Rady Ibrahim Mohamed Mohamed, A novel direct instantaneous torque and flux control with an ADALINE-based motor model for a high performance DD-PMSM, *IEEE Trans. Power Electron.* 22 (5) (2007).
- [2] Ze Wang, Ran Zhou, Chuxiong Hu, Yu Zhu, Online iterative learning compensation method based on model prediction for trajectory tracking control systems, *IEEE Trans. Ind. Inform.* 18 (1) (2022) 415–425.
- [3] Feifei Bu, Fuqiang Xuan, Zhida Yang, Yu Gao, Zihao Pan, Michele Degano, Chris Gerada, Rotor position tracking control for low speed operation of direct-drive PMSM servo system, *IEEE-ASME Trans. Mech.* 26 (2) (2021).
- [4] Y.A.-R.I. Mohamed, A newly designed instantaneous-torque control of direct-drive pmsm servo actuator with improved torque estimation and control characteristics, *IEEE Trans. Ind. Electron.* 54 (5) (2007) 2864–2873.
- [5] Fuli Jin, Jikai Si, Zhiping Cheng, Peng Su, Lianghui Dong, Ge Qi, Analysis of a six-phase direct-drive permanent magnet synchronous motor with novel toroidal windings, in: *Vehicle Power and Propulsion Conference*, 2019.
- [6] A. Tani, M.B. Camara, B. Dakyo, Y. Azzouz, DC/DC and DC/AC converters control for hybrid electric vehicles energy management-ultracapacitors and fuel cell, *IEEE Trans. Ind. Inform.* 9 (2) (2013) 686–696.
- [7] A. Hajizadeh, M.A. Golkar, A. Feliachi, Voltage control and active power management of hybrid fuel-cell/energy-storage power conversion system under unbalanced voltage sag conditions, *IEEE Trans. Energy Convers.* 25 (4) (2010) 1195–1208.
- [8] Anthony M. Gee, Francis V.P. Robinson, Roderick W. Dunn, Analysis of battery lifetime extension in a small-scale wind-energy system using supercapacitors, *IEEE Trans. Energy Convers.* 28 (1) (2013) 24–33.
- [9] Mohamed Bahloul, Shafiuzzaman K. Khadem, Impact of power sharing method on battery life extension in HESS for grid ancillary services, *IEEE Trans. Energy Convers.* PP (99) (2018) 1.
- [10] A.S. Weddell, G.V. Merrett, T.J. Kazimierski, B.M. Al-Hashimi, Accurate supercapacitor modeling for energy harvesting wireless sensor nodes, *IEEE Trans. Circ. Syst. II Express Briefs* 58 (12) (2011) 911–915.
- [11] Phatiphat Thounthong, Stephane Rael, Bernard Davat, Analysis of supercapacitor as second source based on fuel cell power generation, *IEEE Trans. Energy Convers.* 24 (1) (2009) 247–255.
- [12] W. Na, T. Park, T. Kim, S. Kwak, Light fuel-cell hybrid electric vehicles based on predictive controllers, *IEEE Trans. Veh. Technol.* 60 (1) (2011) 89–97.
- [13] M.B. Camara, Daniel Podorean, David Bouquain, Hamid Gualous, Abdellatif Miraoui, Hybrid sources control for electric drives traction applications, in: *International Symposium on Power Electronics, Electrical Drives, Automation and Motion*, 2008, 744–749E-ISBN:978-1-4244-1664-6.
- [14] Ke Jin, Xinbo Ruan, Mengxiang Yang, Min Xu, A hybrid fuel cell power system, *IEEE Trans. Ind. Electron.* 56 (4) (2009) 1212–1222.
- [15] Freek Baalbergen, Pavol Bauer, Jan Abraham Ferreira, Energy storage and power management for typical 4Q-load, *IEEE Trans. Ind. Electron.* 56 (5) (2009) 1485–1498.
- [16] M.B. Camara, H. Gualous, F. Gustin, A. Berthon, Design and new control of DC/DC converters to share energy between supercapacitors and batteries in hybrid vehicles, *IEEE Trans. Veh. Technol.* 57 (5) (2008) 2721–2735.
- [17] J. Moreno, M.E. Ortuzar, J.W. Dixon, Energy-management system for a hybrid electric vehicle, using ultracapacitors and neural networks, *IEEE Trans. Ind. Electron.* 53 (2) (2006) 614–623.
- [18] M.B. Camara, B. Dakyo, H. Gualous, Cristian Nichita, DC/DC converters control for embedded energy management - supercapacitors and battery, in: *Conference of the IEEE Industrial Electronics Society*, 2010.
- [19] Dmitri Vinnikov, Indrek Roasto, Janis Zakis, New bi-directional DC/DC converter for supercapacitor interfacing in high-power applications, in: *Power Electronics and Motion Control Conference (EPE/PEMC)*, 2010 14th International, 2010.
- [20] J. Zakis, D. Vinnikov, I. Roasto, L. Ribickis, Quasi-Z-source inverter based bi-directional DC/DC converter: Analysis of experimental results, in: *Compatibility & Power Electronics*, 2011.
- [21] Janis Zakis, Dmitri Vinnikov, Indrek Roasto, Leonīds Ribickis, Experimental verification of novel bi-directional qZSI based DC/DC converter for short term energy storage systems, *Renew. Energy Power Quality J.* (2011).
- [22] Taehyung Kim, Sangshin Kwak, Jae Do Park, Hybrid system control for robot motors based on a reduced component, multi-voltage power supply system, in: *IEEE Transactions on Circuits and Systems, II. Express briefs*, (68–12) 2021.
- [23] Je Hyun Yi, Woojin Choi, Bo Hyung Cho, Zero-voltage-transition interleaved boost converter with an auxiliary coupled inductor, *IEEE Trans. Power Electron.* (2016) 1.

- [24] Lei Jiang, Chunting Chris Mi, Siqi Li, Chengliang Yin, Jinchuan Li, An improved soft-switching buck converter with coupled inductor, *IEEE Trans. Power Electron.* 28 (11) (2013) 4885–4891.
- [25] Guipeng Chen, Yan Deng, Yong Tao, Xiangning He, Yousheng Wang, Yihua Hu, Topology derivation and generalized analysis of zero-voltage-switching synchronous DC–DC converters with coupled inductors, *IEEE Trans. Ind. Electron.* 63 (8) (2016) 4805–4815.
- [26] Guipeng Chen, Yan Deng, Luan Chen, Yihua Hu, Lin Jiang, Xiangning He, Yousheng Wang, A family of zero-voltage-switching magnetic coupling non-isolated bidirectional DC-DC converters, *IEEE Trans. Ind. Electron.* (2017) 1.
- [27] Mohammad Reza Mohammadi, Hosein Farzanehfard, A new family of zero-voltage-transition nonisolated bidirectional converters with simple auxiliary circuit, *IEEE Trans. Ind. Electron.* 63 (3) (2016) 1519–1527.
- [28] Lei Jiang, Xi Zhang, Chengliang Yin, Chris Mi, Siqi Li, Mengyang Zhang, A novel soft-switching bidirectional DC–DC converter with coupled inductors, in: 2013 Twenty-Eighth Annual IEEE Applied Power Electronics Conference and Exposition, APEC, 2013.
- [29] Yong Zhang, Xu Feng Cheng, Chengliang Yin, Si Cheng, A soft-switching bidirectional DC-DC converter for the battery super-capacitor hybrid energy storage system, *IEEE Trans. Ind. Electron.* (2018) 1.